Materials and Design 115 (2017) 203–212

Contents lists available at ScienceDirect

Materials and Design

journal homepage: www.elsevier.com/locate/matdes

# Microstructure and tribological properties of $Cr_3C_2/Ni_3Al$ composite materials prepared by hot isostatic pressing (HIP)

Lihua Fu [a,b], Wei Han [a], Karin Gong [c], Sven Bengtsson [d], Chaofang Dong [b], Lin Zhao [a,*], Zhiling Tian [a]

[a] Central Iron and Steel Research Institute, Beijing 100081, China
[b] School of Material Science and Engineering, University of Science and Technology Beijing, Beijing 100083, China
[c] Department of Materials and Manufacturing Technology, Chalmers University of Technology, Gothenburg SE-41296, Sweden
[d] Höganäs AB, Höganäs 26383, Sweden

## HIGHLIGHTS

- A $M_7C_3$ (M = Cr, Fe) phase is formed in $Cr_3C_2/Ni_3Al$ composites prepared by hot isostatic pressing.
- The hardness of the $Cr_3C_2/Ni_3Al$ composites increases with increasing addition of $Cr_3C_2$.
- The wear resistance of $Cr_3C_2/Ni_3Al$ composites is improved due to the $Cr_3C_2$ asperities keep the sliding surfaces apart.
- Excess addition of $Cr_3C_2$ (such as 24 vol%) can decrease the wear resistance of $Cr_3C_2/Ni_3Al$ composites.

## GRAPHICAL ABSTRACT

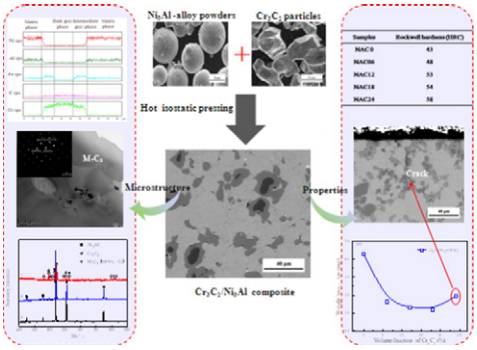


## ARTICLE INFO

*Article history:*
Received 28 September 2016
Received in revised form 14 November 2016
Accepted 15 November 2016
Available online 18 November 2016

*Keywords:*
$Cr_3C_2/Ni_3Al$ composites
Hot isostatic pressing
Microstructure
Tribological properties

## ABSTRACT

$Ni_3Al$-based composites with different $Cr_3C_2$ contents were fabricated by the hot isostatic pressing (HIP) technique. The microstructure, phase constitution, and tribological properties of the composites were investigated by scanning electron microscopy (SEM), energy dispersive spectroscopy (EDS), X-ray diffraction (XRD), transmission electron microscopy (TEM), and pin-on-disk wear tests. The results revealed that the strengthening phase is distributed homogeneously in the $Ni_3Al$ matrix. During the HIP process, $M_7C_3$ (M = Cr, Fe) is formed by diffusion of Fe, C, and Cr to the interface between the $Cr_3C_2$ particles and $Ni_3Al$ matrix. The diffusion process binds the phases and is important for improving the wear resistance of $Cr_3C_2/Ni_3Al$ composites. The wear measurements demonstrated that micro-cutting and fatigue wear are the dominant mechanisms for this tribological pair. The wear resistance of $Cr_3C_2/Ni_3Al$ composites is significantly improved by the addition of $Cr_3C_2$ particles. When the content of $Cr_3C_2$ is within a certain range, the wear resistance of $Cr_3C_2/Ni_3Al$ composites increases as the $Cr_3C_2$ content increases. However, the addition of excess $Cr_3C_2$ (for example, 24 vol% in this work) could lead to a decrease in the wear resistance of the composites. In addition, the average friction coefficients and wear of the counterpart decrease with increasing $Cr_3C_2$ addition.



## 1. Introduction

$Ni_3Al$ is one of the most attractive materials among intermetallic compounds because of its high melting point, low density, high temperature strength, and good creep resistance [1–4]. Furthermore, it has a positive temperature-dependence of strength due to its long-range

* Corresponding author.
*E-mail address:* hhnds@aliyun.com (L. Zhao).

http://dx.doi.org/10.1016/j.matdes.2016.11.060
0264-1275/

ordered crystal structure [5–7]. Therefore, $Ni_3Al$ alloys are considered to be excellent materials for resisting wear at high temperatures. They have been used for tribological applications in which wear-resistance is the main requirement [8–10]. Recent studies have indicated that the high-temperature mechanical strength and hardness of $Ni_3Al$ alloys can be significantly improved by the addition of hard-particle reinforcements [11–13]. When present in iron, cobalt, and nickel matrices, chromium carbide exhibits high hot-hardness and excellent high-temperature oxidation resistance combined with good wetting ability [14–15]. Hence, chromium carbides are chosen frequently as hard-particle reinforcements for addition into $Ni_3Al$-based matrices, to form $Cr_3C_2/Ni_3Al$ composites [8,16]. $Cr_3C_2/Ni_3Al$ composites have been widely investigated as wear-resistant materials in wear applications for many years. Bullock et al. [17] studied directionally solidified Ni-$Ni_3Al$-$Cr_3C_2$ composites and found that the composites show better creep resistance than the matrix-only material. The wear performance of chromium-carbide-reinforced $Ni_3Al$ matrix composites under ambient temperature was studied by Gong et al. [15–16,18]. The results indicated that composites presented better wear resistance compared with the matrix-only material. This was due to the presence of carbide asperities, which kept the sliding surfaces apart during the wear process. Li et al. [19] prepared a $Cr_3C_2/Ni_3Al$ composite coating on steel by welding. A study of the abrasive wear performance of the composite coating showed that the abrasion-resistance of the $Cr_3C_2/Ni_3Al$ composite coating is twice as high as that of the stellite 12 alloy. This can be attributed to the large volume fraction of carbides, high hardness, and good interfacial bonding between the phases. Therefore, it was expected that the unique properties of $Ni_3Al$ alloys and chromium carbides would improve the tribological resistance of materials [11–12,20–21].

Hot isostatic pressing (HIP) is a widely applied powder technique for manufacturing precisely shaped, dense bodies of different types of materials, including metals, ceramics, and others [22–24]. In recent years, it has also been used to produce wear-resistant components for $Cr_3C_2/Ni_3Al$ composites. However, the microstructure and phase constitution of HIP $Cr_3C_2/Ni_3Al$ composite materials have not been investigated systematically in previous studies. The diffusion phenomenon and related phase transformation of $Cr_3C_2/Ni_3Al$ composites during the HIP process have not been clearly understood. It is important to understand the effect of $Cr_3C_2$ content on the microstructure and tribological behavior of $Cr_3C_2/Ni_3Al$ composites processed by the HIP technique, for practical applications as well as academic research.

In this paper, $Ni_3Al$-based composites with various $Cr_3C_2$ contents were prepared using the hot isostatic pressing technique. The microstructure and phase constitution of the HIP $Cr_3C_2/Ni_3Al$ composites were characterized by field emission scanning electron microscopy (SEM), energy dispersive spectroscopy (EDS), X-ray diffraction (XRD), and transmission electron microscopy (TEM). Moreover, the tribological properties of the composite materials were investigated, and the influence of $Cr_3C_2$ content on the wear behavior of the composites was analyzed.

## 2. Experimental details

### 2.1. Materials

$Ni_3Al$-alloy powders (~40–100 μm) with a chemical composition (wt%) of Ni-9.87 Al- 11.63 Fe-0.50 Mn-0.50 Ti-0.2 B and $Cr_3C_2$ particles (~20 μm, 99.5% purity) were selected as the raw materials. Powders of the $Ni_3Al$ alloy were supplied by the Chalmers University of Technology, where they were synthesized using vacuum melting and inert gas atomization technology. The powders were first mechanically mixed with $Cr_3C_2$ particles in a roller ball mill. The mixing process was carried out at a rotational speed of 50 rpm for 24 h. In this work, the $Ni_3Al$-alloy powders were uniformly mixed with 6 vol%, 12 vol%, 18 vol%, and 24 vol% of $Cr_3C_2$ particles, respectively. Then, the mixed powders were processed by the HIP method at 1160 °C and 140 MPa for 3 h to obtain the $Cr_3C_2/Ni_3Al$ composites (NAC06, NAC12, NAC18, NAC24). As a reference for comparison, a monolithic $Ni_3Al$-alloy (NAC0) without $Cr_3C_2$ powders was also fabricated.

### 2.2. Characterization and wear tests

The microstructure of the monolithic $Ni_3Al$-alloy and its composites was observed by SEM and EDS (NOVA NANOSEM 450). The phases of the $Cr_3C_2/Ni_3Al$ composites were analyzed by XRD (D8 ADVANCE) and TEM (JEM-2010). In order to avoid interference from the signal of the matrix phase in the XRD pattern, chromium carbides were extracted from the $Cr_3C_2/Ni_3Al$ composites by constant-current electrolysis. This process was carried out in an electrolytic solution of 1.6 mol/L hydrochloric acid, 0.7 mol/L propanetriol, 0.04 mol/L citric acid, and methanol solution for 3 h, with a constant current density of approximately 50 $mA/cm^2$. Samples for TEM were firstly mechanically thinned down to 10– 20 μm in thickness. Then, the foils were ion-milled using an ion polishing system (Leica RES 101). The ion-milling process consisted of two steps: in the first step, the foils were milled at an incidence angle of 8° under an accelerating voltage of 5 kV for 3 h; in the second step, the samples were continuously thinned under an incidence angle of 3° and accelerating voltage of 3 kV for 1 h. The hardness of the $Ni_3Al$-alloy and $Cr_3C_2/Ni_3Al$ composites was measured using a HRS-150 Rockwell hardness instrument with a load of 150 kg and indentation time of 10 s. Each measurement was conducted three times to verify the reproducibility of the results. The equivalent Vickers hardness was estimated using conversion tables. The pin-on-disk wear tests were performed using an Optimal SRV®4 reciprocal friction and wear tester at room temperature. The pins were composed of the monolithic $Ni_3Al$-alloy and $Cr_3C_2/Ni_3Al$ composites, with dimensions of 3 × 2 × 14 mm. The face with an area of 3 × 2 mm was chosen as the wear surface to be brought into contact with the counterpart disk. The counterpart disk (Ø24 × 7.88 mm) was made of gray cast iron with the chemical composition (wt%) of Fe-3.20 C-1.10 Si-0.80 Mn-0.07 S-0.2 P-1.0 Cu-0.22 V. Before the tribological measurements, all pins and counterpart disks were polished with 1500 grit SiC paper, then rinsed with deionized water, and finally, degreased by acetone. The tribological tests were carried out under a load of 48 N, a stroke of 1.0 mm, a frequency of 50 Hz, and a testing time of 60 min. The mass loss by wear was calculated using the masses of each sample before and after the wear tests. More than three samples were tested for each test condition, and the average value was used. Dividing by the density of each sample, mass loss by wear was converted into volume loss by wear. The data used for the conversion are as follows: the density of the $Ni_3Al$-alloy was 7.5 $g/cm^3$, the density of the $Cr_3C_2$ particles was 6.68 $g/cm^3$, and the density of gray cast iron was 7.2 $g/cm^3$.

## 3. Results

### 3.1. Microstructure and phase constitution of the composite materials

Fig. 1 shows the microstructure of the $Ni_3Al$-alloy and $Cr_3C_2/Ni_3Al$ composites with various $Cr_3C_2$ contents. As shown in Fig. 1(a), the NAC-alloy exhibits a fairly homogeneous structure. In Fig. 1(b)–(e), it can be observed that the chromium carbides, which form the strengthening phase of the composites, are uniformly dispersed in the matrix. Moreover, the proportion of the strengthening phase in the composites increases with increasing addition of $Cr_3C_2$. Fig. 1(f) reveals that the $Cr_3C_2/Ni_3Al$ composites mainly consist of a dark gray phase, an intermediate gray phase, and a light gray phase, as illustrated in the backscattered electron image. EDS analysis was conducted in order to determine the chemical composition of these three phases, and the results as shown in Fig. 2. Only chromium and carbon were found in the energy spectrum of the dark gray phase (see Fig. 2(a)). In the intermediate gray phase (see Fig. 2(b)), iron and a small amount of nickel were also found in addition to chromium and carbon. Nickel was dominant in

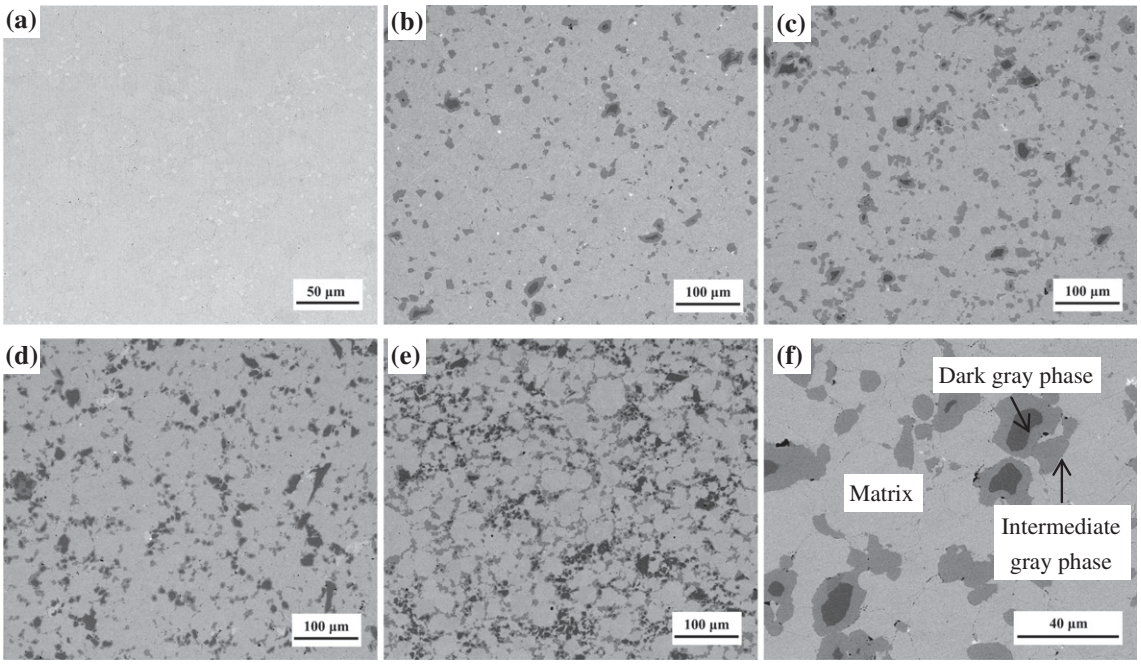


**Fig. 1.** Back-scattered electron images of the microstructure of $Ni_3Al$-alloy and $Cr_3C_2/Ni_3Al$ composites: (a) sample NAC0; (b) sample NAC06; (c) sample NAC12; (d) sample NAC18; (e) sample NAC24; (f) high magnification for sample NAC12.

the matrix, with smaller amounts of aluminum, iron, and traces of chromium and carbon. In order to obtain more information about the continuous distribution of each element over the phase interfaces, EDS line scanning analysis was performed across the chromium carbide particles. As shown in Fig. 3, the changes in distribution of Ni, Al, Cr, and Fe elements at the interface are clearly observed. Nickel and aluminum were mostly found in the matrix. The iron content was significantly higher in the intermediate gray phase but was lower in the matrix phase. The carbon signal was higher in the dark gray phase, lower in the intermediate gray phase, and very low in the matrix phase. However, the poor precision of the carbon signal in the EDS analysis prevents any definite conclusions from these variations. The chromium signal was the highest in the dark gray phase, somewhat lower in the intermediate phase, and very low in the matrix phase.

Fig. 4(a) and (b) present the X-ray diffraction patterns of the $Ni_3Al$-alloy and $Cr_3C_2/Ni_3Al$ composites. The results reveal that the $Ni_3Al$-alloy and $Cr_3C_2/Ni_3Al$ composite matrices have a $Ni_3Al$ crystal structure, with peak signals at $2\theta = 43.6°$, 50.8°, and 74.8°. The diffraction patterns of $Cr_3C_2/Ni_3Al$ composites do not show obvious signals for carbides, which is attributed to interference from the strong peak of $Ni_3Al$.

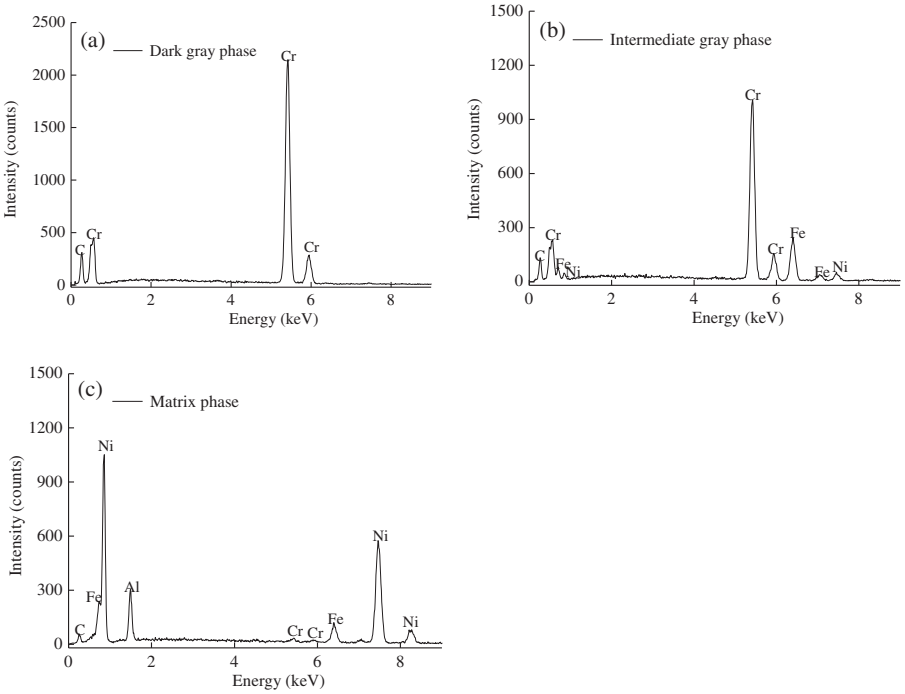


**Fig. 2.** EDS analysis of the three phases in $Cr_3C_2/Ni_3Al$ composites: (a) dark gray phase; (b) intermediate gray phase; (c) matrix phase.

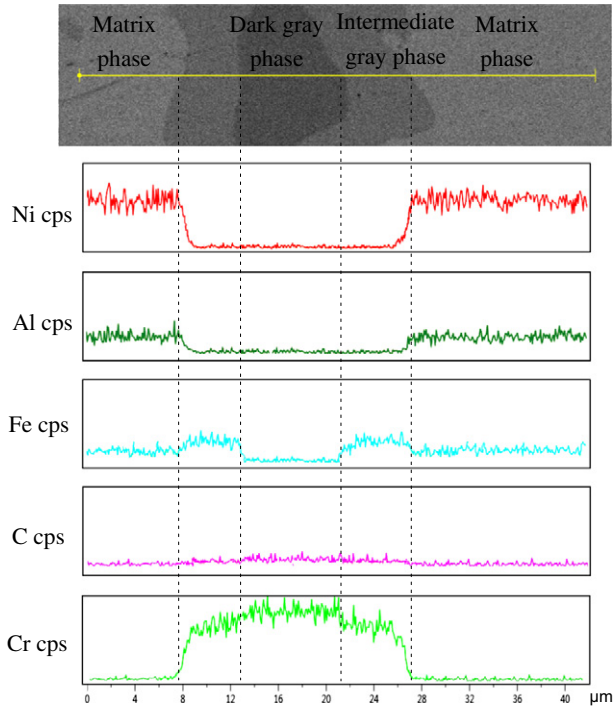


**Fig. 3.** EDS line scanning analysis across a carbide particle of sample NAC12.

Therefore, for the X-ray diffraction analysis in our work, chromium carbides were extracted from the $Cr_3C_2/Ni_3Al$ composites. The XRD pattern of the carbide extract (see Fig. 4(c)) indicates that two phases exist in the composites, namely, $Cr_3C_2$ and $M_7C_3$ (M = Cr or Fe). TEM was applied to determine the phase structure of the composites. Fig. 5(a) and (b) show TEM images of the matrix phase and the intermediate gray phase, respectively. Fig. 5(c) and (e) show the electron diffraction pattern and EDS spectrum of the matrix phase in Fig. 5(a). The electron diffraction pattern in Fig. 5(c) exhibits the $[0\bar{1}\bar{1}]$ zone axis of the $Ni_3Al$ fcc structure, and its chemical composition coincides with the EDS results of the matrix, mentioned above. Fig. 5(d) and (f) show the electron diffraction pattern and EDS spectrum of the intermediate gray phase in Fig. 5(b). The results suggest that Fig. 5(d) shows a $[0\bar{2}12]$ zone axis pattern of the $M_7C_3$ hcp structure, which mainly consists of Cr, C, Fe and Ni elements.

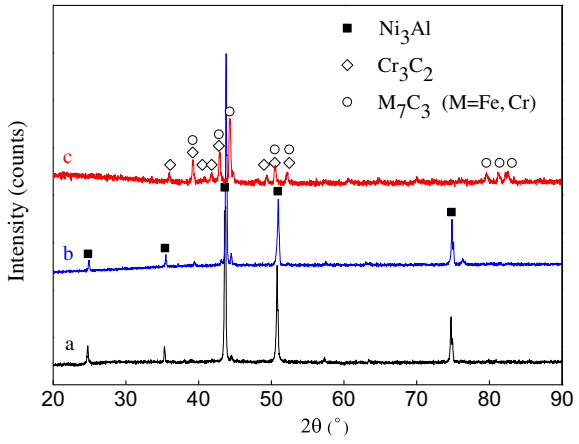


**Fig. 4.** XRD pattern of (a) $Ni_3Al$-alloy; (b) NAC12 composites and (c) carbide extract of sample NAC12.

### 3.2. Hardness and tribological properties of the composite materials

Rockwell hardness measurements were conducted on the samples NAC0, NAC06, NAC12, NAC18, and NAC24. Table 1 lists the Rockwell hardness of samples and their equivalent Vickers hardness values. It can be observed that the hardness of the $Ni_3Al$-alloy is approximately 43 HRC. When 6 vol% $Cr_3C_2$ was added into the materials, the hardness of the $Cr_3C_2/Ni_3Al$ composites was significantly improved to approximately 48 HRC. When 24 vol% $Cr_3C_2$ was added, the hardness of the $Cr_3C_2/Ni_3Al$ composite increased to 58 HRC. These results suggest that the hardness of the $Cr_3C_2/Ni_3Al$ composites increases with increasing addition of $Cr_3C_2$. In fact, the improvement in hardness of the $Cr_3C_2/Ni_3Al$ composites is not only because of the added hard $Cr_3C_2$ particles but also due to the diffusion of Cr into the matrix material, resulting in a solution hardening effect on the $Ni_3Al$ matrix.

Fig. 6 shows the variation of average friction coefficients of the samples as a function of $Cr_3C_2$ content. It is clear that the average friction coefficient of the $Ni_3Al$-alloy is approximately 0.85. The friction coefficient of the composites decreased with increasing addition of $Cr_3C_2$. Finally, the friction coefficient of the composites dropped to ~0.5 for the specimen NAC24, which had 24 vol% $Cr_3C_2$ added to it. The volume losses by wear of the $Ni_3Al$-alloy and composites with different $Cr_3C_2$ contents are given in Fig. 7(a). The wear rate of the monolithic $Ni_3Al$-alloy was quite high. However, the volume loss by wear decreased remarkably for the sample with 6 vol% $Cr_3C_2$-addition. It was less than half of the volume loss of the monolithic $Ni_3Al$-alloy. The volume loss by wear of the composites was the lowest (0.24 $mm^3$) for 18 vol% $Cr_3C_2$ addition. However, it then increased (0.4 $mm^3$) when the $Cr_3C_2$ content was 24 vol%. Fig. 7(b) presents the volume loss by wear of the counterpart disk (gray cast iron) for different composites. Fig. 7(b) shows that the damage to the counterpart disk by the $Cr_3C_2/Ni_3Al$ composites decreased as the $Cr_3C_2$ content was increased, resulting in a reduction in the wear rate of the counterpart material.

## 4. Discussion

### 4.1. Microstructure and phase constitution of the composite materials

The observed microstructure reveals that the $Cr_3C_2/Ni_3Al$ composites are composed of three phases. The XRD and TEM analyses indicate that the matrix phase is $Ni_3Al$, the intermediate gray phase (as seen in Fig. 1(f)) has a $M_7C_3$ (M = Cr, Fe) structure, while the dark gray phase (in Fig. 1(f)) is $Cr_3C_2$ that has not been transformed during the HIP process. It is estimated that the $Ni_3Al$ has a long-range ordered crystal structure that is stable up to temperatures near its melting point (1390 °C). The temperature of the HIP process in this study is approximately 1160 °C. Therefore, the matrix phase retains the $Ni_3Al$ crystal structure.

The melting temperature of $Cr_3C_2$ is approximately 1890 °C. However, some studies have indicated that surface diffusion of chromium atoms from $Cr_3C_2$ carbide into the nickel matrix in the $Cr_3C_2$–Ni system takes place at a relatively low temperature (approximately 700–800 °C) [25]. As the temperature is raised, the diffusion reaction becomes more vigorous. When the temperature is raised to 900–980 °C, the $Cr_3C_2$ carbide partially decomposes into free graphite and chromium atoms, which diffuse into the matrix [25]. Therefore, when the experimental temperature was raised to 1160 °C in this study, the $Cr_3C_2$ particles may have fully or partially decomposed into the graphite and Cr atoms, and diffused into the $Ni_3Al$ matrix materials. In addition, Fe and Ni atoms from the $Ni_3Al$ phase can also diffuse into the carbides (as shown in the EDS results, see Fig. 2). Moreover, the Fe atoms move by an uphill diffusion process (see Fig. 3) because of the reaction with carbon, which can reduce the chemical potential. During the cooling process, the dissolved Cr and C atoms may resolidify into a more stable structure. It is well known that Cr and C may form several different stable carbides, namely, $Cr_3C_2$, $Cr_7C_3$, and $Cr_{23}C_6$. The thermodynamic

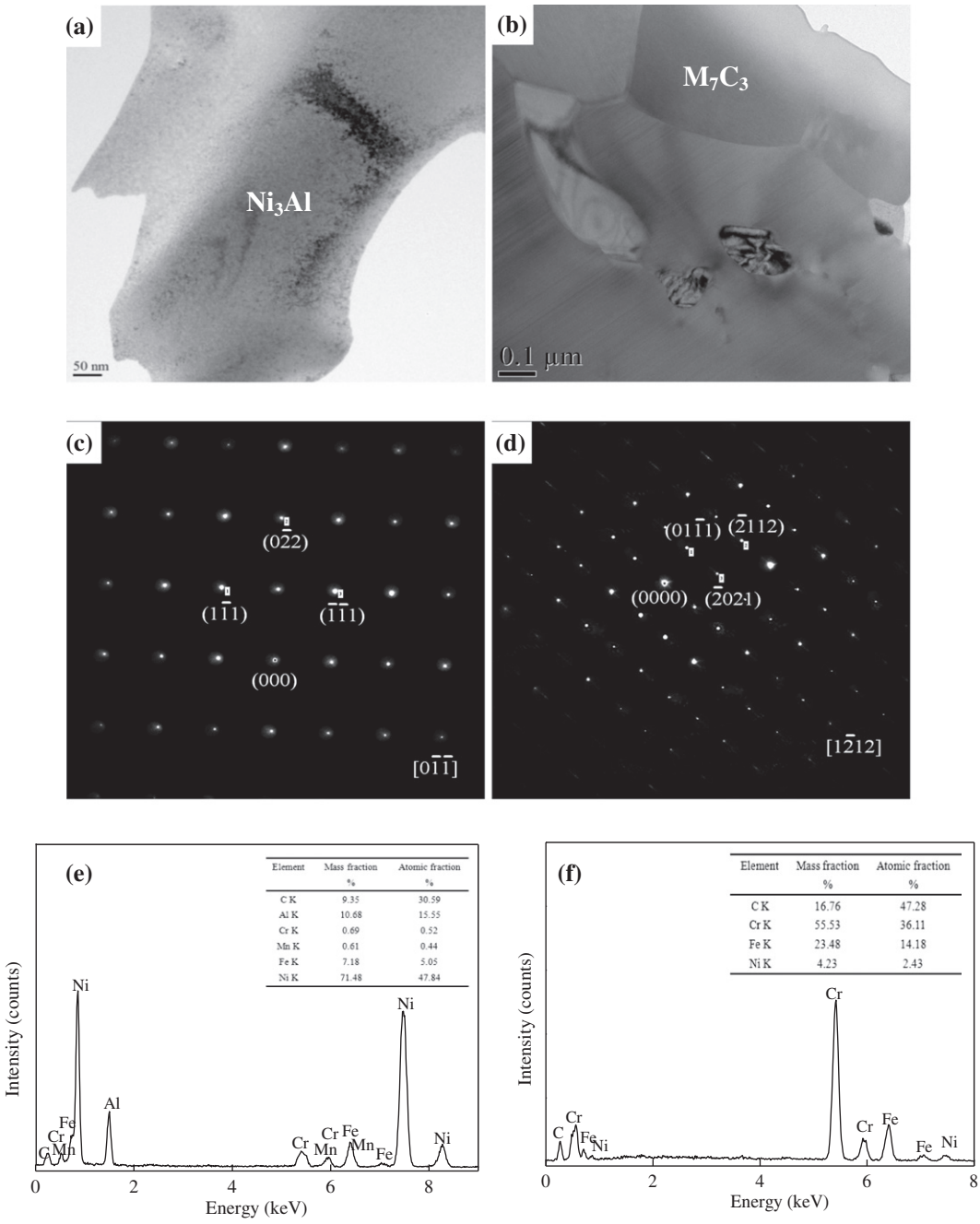


**Fig. 5.** TEM results of matrix phase and intermediate gray phase in NAC12 composites: (a) TEM image of matrix phase; (b) TEM image of intermediate gray phase; (c) electron diffraction patterns of matrix phase; (d) electron diffraction patterns of intermediate gray phase; (e) chemical composition of matrix phase; (f) chemical composition of intermediate gray phase.

equations for the standard Gibbs energy of formation ($\Delta G_f^o$) of these carbides are [26]:

$$\Delta G_f^o(Cr_3C_2) = -54344 - 19.57\,T(\pm 9400)\ \text{J/mol} \quad (1)$$

$$\Delta G_f^o(Cr_7C_3) = -92067 - 41.5\,T(\pm 2800)\ \text{J/mol} \quad (2)$$

$$\Delta G_f^o(Cr_{23}C_6) = -236331 - 86.2\,T(\pm 10000)\ \text{J/mol} \quad (3)$$

Substituting the experimental temperature (T) in the expression above, the standard Gibbs energies of formation ($\Delta G_f^o$) of $Cr_3C_2$, $Cr_7C_3$, and $Cr_{23}C_6$ are about −82.4 kJ/mol, −151.5 kJ/mol, and −359.9 kJ/mol, respectively. According to the standard Gibbs energy of formation ($\Delta G_f^o$), $Cr_{23}C_6$ carbide has the highest tendency of formation from dissolved Cr and C. However, the XRD analysis and TEM results detected the $M_7C_3$ (M = Cr, Fe) structure instead of the $M_{23}C_6$ (M = Cr, Fe) structure in this work. This is because the reaction is not only influenced by thermodynamic factors but also depends on kinetic

**Table 1**
Hardness of $Ni_3Al$-alloy and $Cr_3C_2/Ni_3Al$ composites.

| Samples | Rockwell hardness (HRC) | Equivalent Vickers hardness (HV) |
|---|---|---|
| NAC 0 | 43 | 411 |
| NAC06 | 48 | 470 |
| NAC12 | 53 | 570 |
| NAC18 | 54 | 597 |
| NAC24 | 58 | 666 |

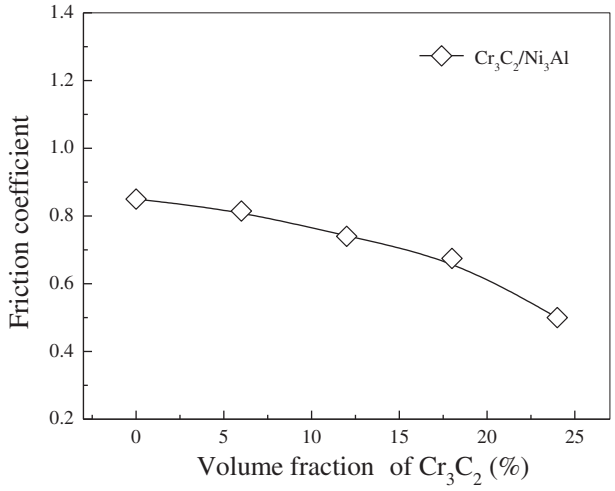


**Fig. 6.** Average friction coefficients of $Ni_3Al$-alloy and $Cr_3C_2/Ni_3Al$ composites.

factors. On the other hand, the above Gibbs' free energy calculations are based on a pure Cr-C system. In fact, the Cr and C atoms on the outer edges of $Cr_3C_2$ particles diffuse and dissolve into the matrix, resulting in a disturbed Cr/C ratio at the dissolved region of carbide. Additionally, some iron and a small amount of nickel diffuse into the dissolved region of the carbide, altering the thermodynamic equilibria for the formation of chromium carbides. Considering the existence of the Fe element, the isothermal section diagrams of the Fe-Cr-C system at 1160 °C and 900 °C are shown in Fig. 8. The chemical composition (as seen in Fig. 5(f)) of the intermediate gray phase suggests that the atomic fractions of Cr, C, Fe, and Ni elements are 36.11, 47.28, 14.18, and 2.43, respectively. This chemical composition is located just inside the region corresponding to $M_7C_3$ + C(Graphite) in the isothermal section diagrams at 1160 °C and 900 °C, as shown by the solid circle in Fig. 8. Therefore, the $M_7C_3$ (M = Cr, Fe) structure is detected in the diffusion phase. This result is also consistent with results in the literature [25,27–28]. The size of the $Cr_3C_2$ particles is quite large. Most particles are not completely decomposed during the high-temperature period. The carbide core, i.e., the dark gray phase, still retains the $Cr_3C_2$ structure after the cooling process.

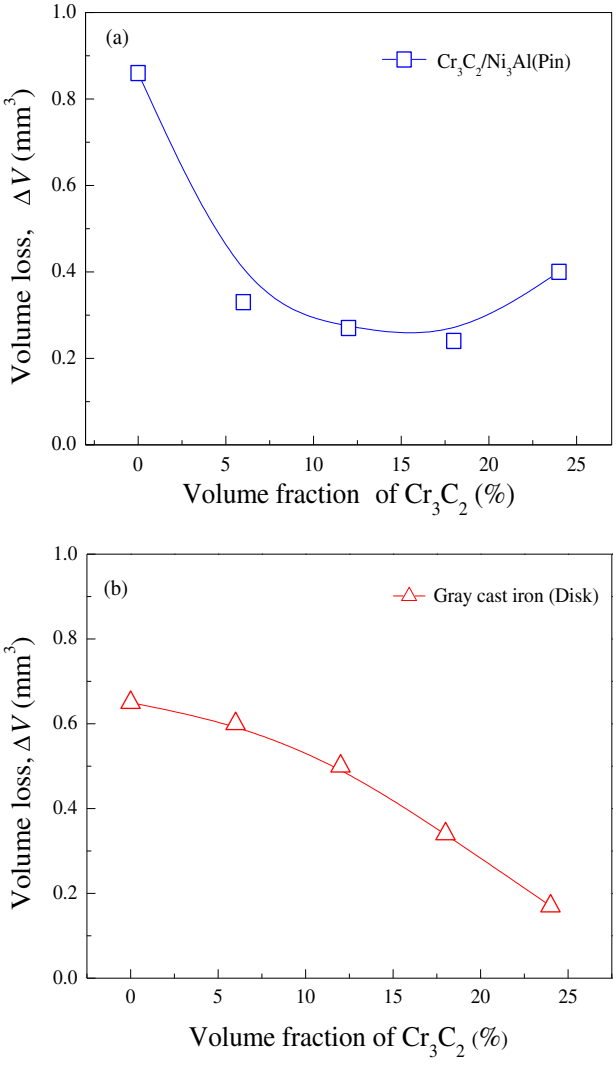


**Fig. 7.** Volume loss by wear of samples: (a) $Ni_3Al$-alloy and $Cr_3C_2/Ni_3Al$ composites; (b) their counterpart disks.

### 4.2. Wear resistance of the composite materials

Fig. 9 shows the back-scattered electron images of the worn surfaces of the $Ni_3Al$-alloy and $Cr_3C_2/Ni_3Al$ composites with various $Cr_3C_2$ contents. The results suggest that many layers of wear debris cover the surface of NAC0, as shown in Fig. 9(a). Parallel grooves on the worn surface of NAC06 are found in Fig. 9(b). However, the quantity of wear debris is

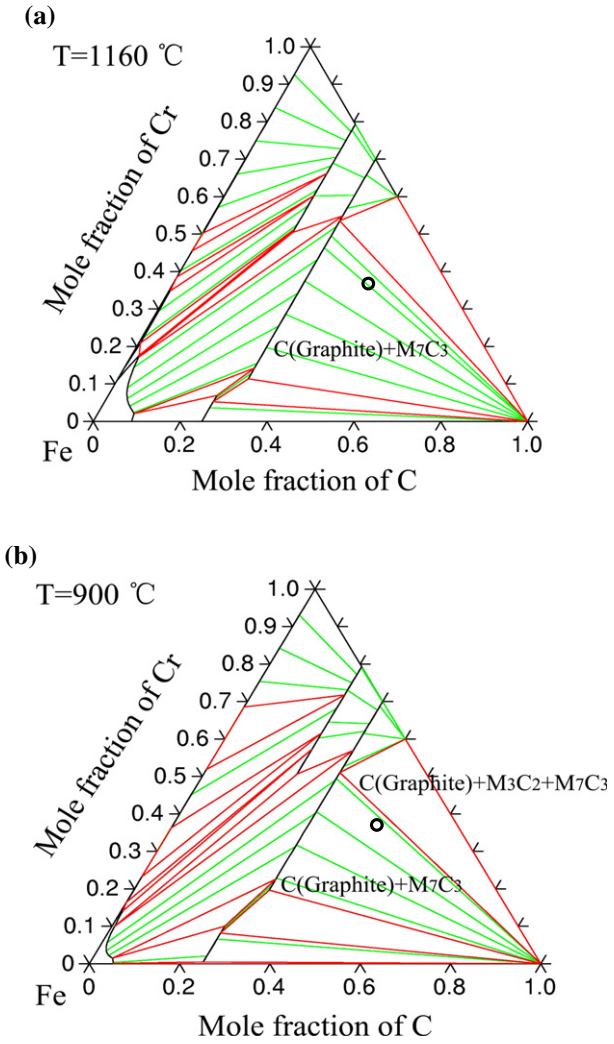


**Fig. 8.** Isothermal section diagrams of the Fe-Cr-C system at (a)1160 °C and (b)900 °C.

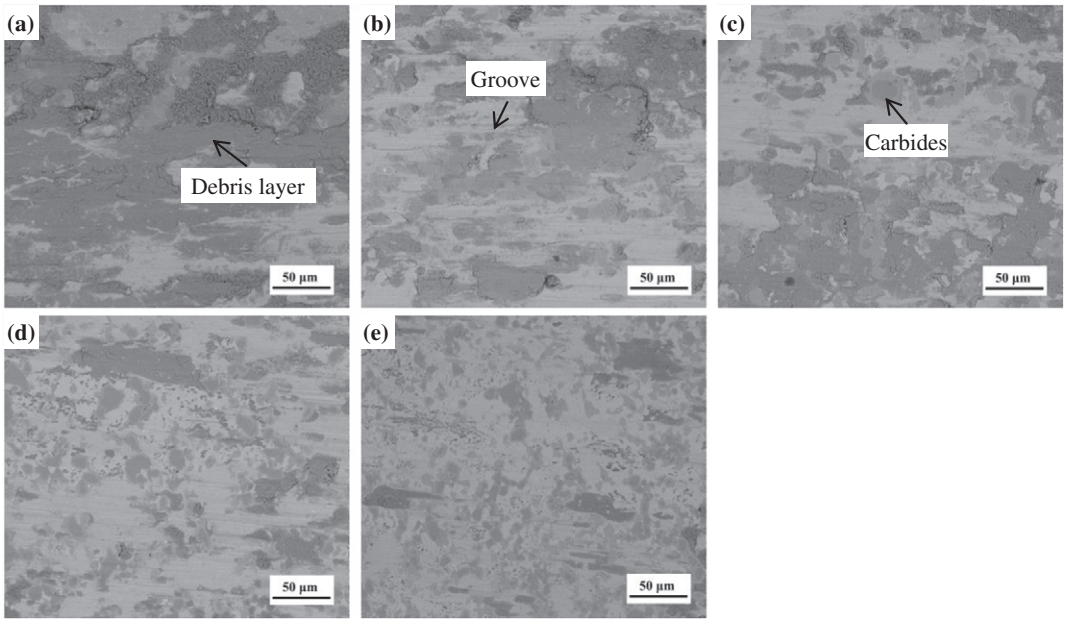


**Fig. 9.** Back-scattered electron images of the worn surface morphologies of $Ni_3Al$-alloy and $Cr_3C_2/Ni_3Al$ composites: (a) sample NAC0; (b) sample NAC06; (c) sample NAC12; (d) sample NAC18; (e) sample NAC24.

decreased in sample NAC06. With increasing $Cr_3C_2$ addition (see Fig. 9(c)–(e)) the amount of wear debris decreases. Furthermore, the grooves are increasingly shallow and are even interrupted near the chromium carbide particles. It is well known that the development and survival of the layers of wear debris is associated with many factors, including the depth of grooves, ductility of the material, chemical affinity of the surface, etc. In this case, it is reasonable that the debris particles adhere with greater difficulty to hard $Cr_3C_2$ particles rather than the ductile matrix. Deeper grooves are not easy to form as more $Cr_3C_2$ is added. Therefore, it is difficult to form layers of wear debris on the surfaces of samples with high $Cr_3C_2$ contents. Fewer debris layers are found on the surfaces of composites with high $Cr_3C_2$ contents. The analysis of average friction coefficients of samples showed that samples with high $Cr_3C_2$ contents have relatively low friction coefficients, as shown in Fig. 6. This low friction could be attributed to the decrease in debris layers on the surfaces of these materials. Similar results have been reported in related literature [29]. Although a detailed analysis of this result was not conducted in this work, it can be studied in our further work.

The characteristics of worn surfaces reported above may indicate that micro-cutting wear is the dominant mechanism occurring on the surface of the $Ni_3Al$-based composite materials. The micro-cutting effect is weakened when the $Cr_3C_2$ content in the composites is increased. Previous works [16,18] have studied the wear mechanism of the $Ni_3Al$ alloy. They noted that a wear-resistant sub-surface layer forms first under the worn surface of the $Ni_3Al$ alloy, due to its plastic deformation and strain-hardening. Then, the sub-surface layer may break into filings and fall off from the worm surface in the following wear process. Finally, these filings will act as wear debris particles and cause micro-cutting of

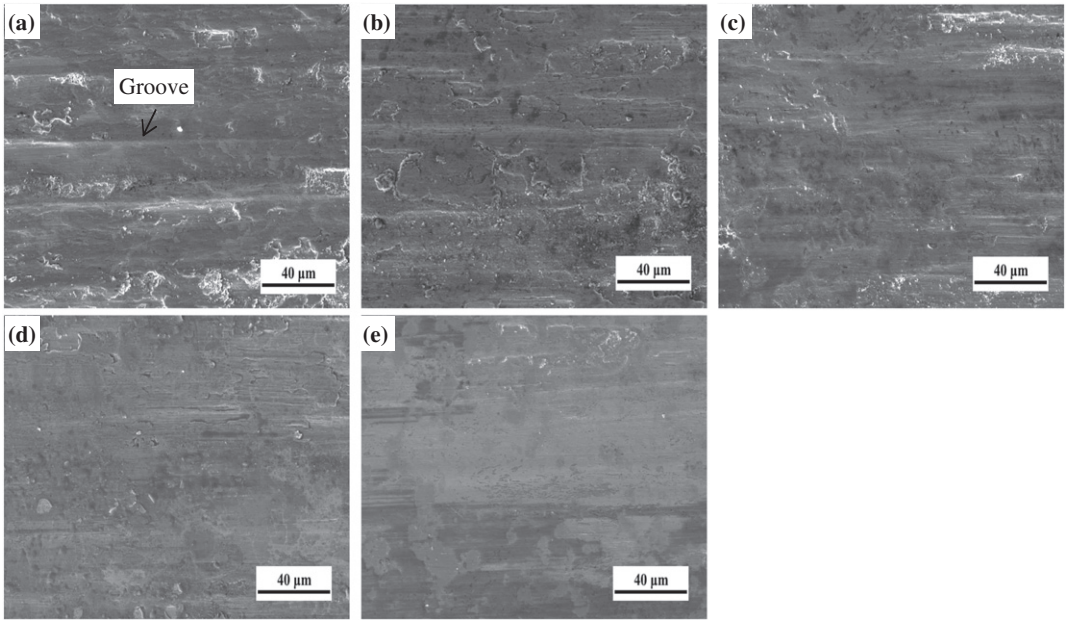


**Fig. 10.** Secondary electron images of the worn surfaces of $Ni_3Al$-alloy and $Cr_3C_2/Ni_3Al$ composites: (a) sample NAC0; (b) sample NAC06; (c) sample NAC12; (d) sample NAC18; (e) sample NAC24.

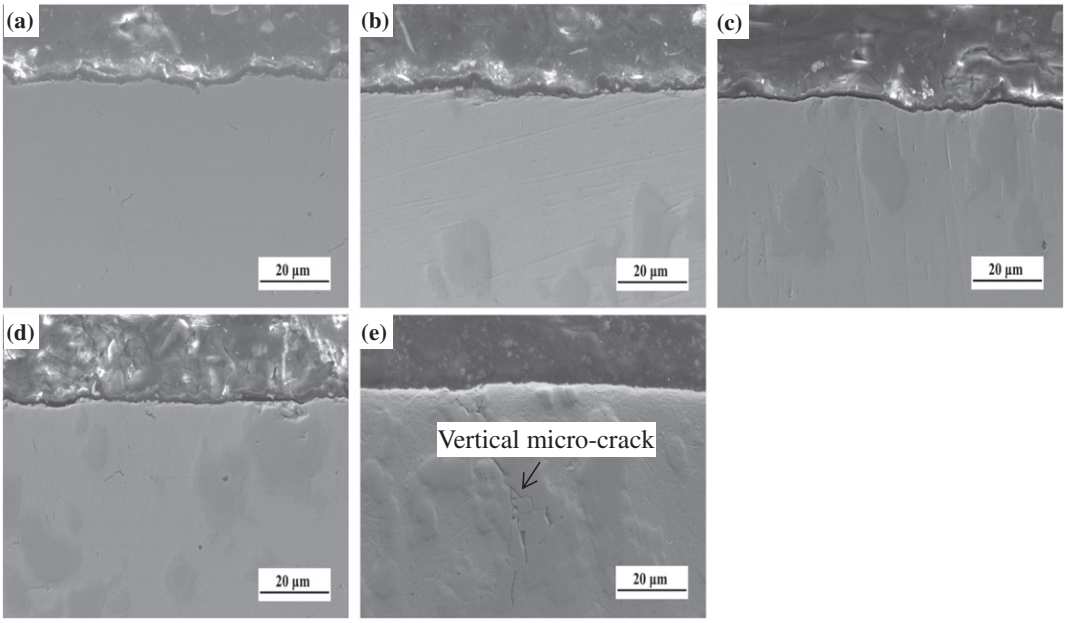


**Fig. 11.** Cross-sectional morphologies after wear testing of $Ni_3Al$-alloy and $Cr_3C_2/Ni_3Al$ composites: (a) sample NAC0; (b) sample NAC06; (c) sample NAC12; (d) sample NAC18; (e) sample NAC24.

the surface of materials. Based on the wear process for the $Ni_3Al$ alloy, the $Cr_3C_2$ particles added to the composites may impact their wear behaviors in the following ways: on the one hand, the hard $Cr_3C_2$ asperities in the surface separate the sliding surfaces and avoid direct contact between the composite testing material and the disk; on the other hand, the thickness of the sub-surface layer is decreased and the size of the wear debris particles is smaller because the hardness of the composites is increased by the $Cr_3C_2$ particles. In addition, the carbide strengthening phase in the $Cr_3C_2/Ni_3Al$ composites may block the cutting process of the wear debris particles. Therefore, the micro-cutting effect is reduced and the grooves are gradually shallowed by the addition of $Cr_3C_2$ particles in the composites. These phenomena are so clearly visible in the secondary electron images of the worn surfaces of $Ni_3Al$-alloy and $Cr_3C_2/Ni_3Al$ composites, as shown in Fig. 10. Because of this, the wear loss of $Cr_3C_2/Ni_3Al$ composites decreases with increasing $Cr_3C_2$ addition for a certain range of $Cr_3C_2$ content, as shown in Fig. 7(a). But, there is an unexpected increase in the volume loss of sample NAC24 with 24 vol% $Cr_3C_2$. Zhu et al. [30] suggested that optimal addition of $Cr_3C_2$ can improve the strength of materials, but excess $Cr_3C_2$ addition could lead to a decrease in strength. In this study, cross-sectional observations of pins were recorded after wear testing. As shown in Fig. 11, there are no micro-cracks below the worn surfaces of samples NAC0, NAC06, NAC12, and NAC18, but there are obvious cracks in sample NAC24. The results indicate that excess $Cr_3C_2$ addition (such as 24 vol%) results in the formation of vertical micro-cracks even after wear testing (as shown in Fig. 11 (e)). Therefore, the volume loss by wear is lowest for NAC18, which has 18 vol% $Cr_3C_2$ content, while that of NAC24 with 24 vol% $Cr_3C_2$ content is worse.

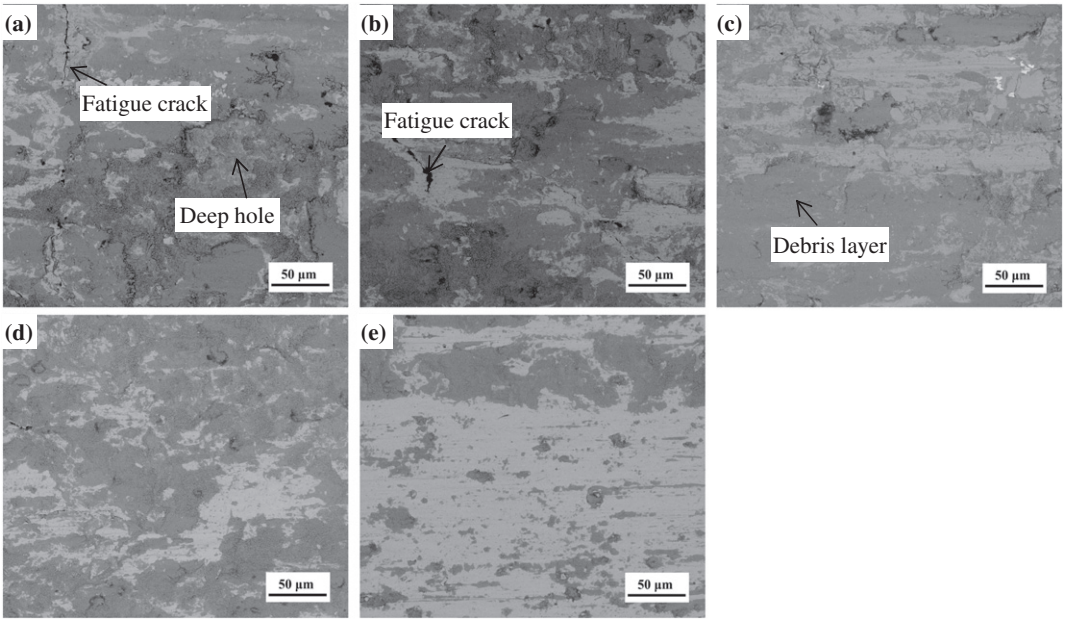


**Fig. 12.** Worn surface morphologies of the counterpart disks of $Ni_3Al$-alloy and $Cr_3C_2/Ni_3Al$ composites: (a) sample NAC0; (b) sample NAC06; (c) sample NAC12; (d) sample NAC18; (e) sample NAC24.

**Table 2**
Chemical composition (wt%) of wear debris for tested samples.

| Samples | Fe | Si | O | Ni | Al | Cr |
|---|---|---|---|---|---|---|
| NAC 0 | 36.3 | 0.4 | 15.7 | 41.6 | 3.7 | – |
| NAC06 | 40.5 | 0.3 | 14.4 | 35.8 | 3.2 | 3.2 |
| NAC12 | 48.2 | 0.4 | 19.6 | 23.9 | 2.0 | 4.1 |
| NAC18 | 63.2 | 0.7 | 16.2 | 15.1 | 0.7 | 2.0 |
| NAC24 | 16.0 | – | 17.9 | 39.8 | 5.3 | 18.2 |

The worn surface morphologies of the counterpart disk of the $Ni_3Al$-alloy and $Cr_3C_2/Ni_3Al$ composites with various $Cr_3C_2$ contents are given in Fig. 12. From these figures, some fatigue cracks can be found on the surface of the counterpart disk for the samples NAC0 and NAC06. The counterpart disk for sample NAC0 even exhibits some spalling. As the $Cr_3C_2$ content in the $Ni_3Al$-based composites is increased, the fatigue cracks on their disks become less obvious and the amount of wear debris layers decreases progressively. This is because the initiation and propagation of cracks on the worn surfaces is associated with shear stresses on the contacting surfaces and the frequency of cycle stress [31]. However, shear stresses are caused by friction, which is related to the layer of debris on the contacting surfaces in this work. Fig. 9 and Fig. 12 show that the quantity of debris layers on the surfaces of both pins and disks decreases with increasing $Cr_3C_2$ content in the composites. Therefore, shear stresses on the worn surfaces of disks are reduced by the addition of $Cr_3C_2$. Decreasing shear stress on the surface should lower the risk of crack initiation and propagation on the surface of the disk, thus decreasing wear of the disk. This also explains why volume loss by wear results from the disk.

Table 2 shows the chemical composition of the wear debris from different samples. The results indicate that the wear debris is composed of a mixture of the $Cr_3C_2/Ni_3Al$ composites and their counterpart disks. The debris from tests on NAC0 and NAC24 contains a higher weight percentage of nickel which mainly originates from the composites, compared to iron which mainly originates from the counterpart disk. This suggests that the volume loss of NAC0 and NAC24 composites is more severe compared to the wear of their respective counterpart disks. Coincidentally, the volume loss by wear of the NAC0 (0.84 $mm^3$) and NAC24 (0.4 $mm^3$) composites is higher than the wear of their respective counterpart disks (0.65 $mm^3$ and 0.17 $mm^3$) in Fig. 9.

## 5. Conclusions

$Ni_3Al$-based composite materials with different $Cr_3C_2$ contents were fabricated by the hot isostatic pressing (HIP) technique. The microstructure and phase constitution of the $Cr_3C_2/Ni_3Al$ composite materials revealed that the chromium carbide strengthening phase is distributed homogeneously in the $Ni_3Al$ matrix, and the proportion of the strengthening phase in the composites increases with increasing $Cr_3C_2$ addition. During the HIP process, the $M_7C_3$ (M = Cr, Fe) phase is formed in the $Cr_3C_2/Ni_3Al$ composites, due to diffusion and recrystallization at the interface between the $Cr_3C_2$ particles and $Ni_3Al$ matrix. Therefore, $Cr_3C_2/Ni_3Al$ composite materials are mainly composed of partially dissolved $Cr_3C_2$ particles, with the $M_7C_3$ (M = Cr, Fe) phase forming at the interface between the original particles and the $Ni_3Al$ matrix phase. The $Ni_3Al$ and $Cr_3C_2$ phases in the $Ni_3Al$-based composites create a strong diffusion bond via the formed $M_7C_3$ (M = Cr, Fe) diffusion phase.

The hardness of the $Cr_3C_2/Ni_3Al$ composites increases with increasing $Cr_3C_2$ addition, which is attributed to the high hardness of $Cr_3C_2$ particles and the solid solution strengthening effect of chromium in the matrix phase. Under specified friction and wear conditions, the wear resistance of $Cr_3C_2/Ni_3Al$ composites is significantly improved with increasing addition of $Cr_3C_2$, within a certain range of $Cr_3C_2$ content. However, further increase in $Cr_3C_2$ content (such as 24 vol% in this work) results in a decrease in wear resistance because of the decrease in strength. Moreover, damage to the counterpart disks of the $Cr_3C_2/Ni_3Al$ composites decreases as the $Cr_3C_2$ content is increased. The observations of worn surface morphologies suggest that micro-cutting and fatigue wear are the dominant mechanisms for this tribological pair.

## Acknowledgments

This study was financially supported by the International Science and Technology Cooperation Program of China (Nos. 2015DFA50970 and 2012DFG51670) and the Tribology Science Fund of the State Key Laboratory of Tribology (No. SKLTKF14B11).

## References

[1] J.X. Wang, J.H. Qian, X.J. Zhang, Y.Q. Wang, Research status and progress of NiAl based alloys as high temperature structural materials, Rare Metals 30 (2011) 422–426.
[2] P. Jozwik, W. Polkowski, Z. Bojar, Applications of $Ni_3Al$ based intermetallic alloys-current stage and potential perceptivities, Materials 8 (2015) 2537–2568.
[3] X. Chen, J.F. Xu, Q.Q. Sun, W. Yang, W.H. Xiong, Characterization of intermetallic bonded TiC composites prepared by mechanically induced self-sustained reaction, Mater. Des. 89 (2016) 102–108.
[4] L. Wu, J. Yao, H.X. Dong, Y.H. He, N.P. Xu, J. Zou, B.Y. Huang, C.T. Liu, The corrosion behavior of porous $Ni_3Al$ intermetallic materials in strong alkali solution, Intermetallics 19 (2011) 1759–1765.
[5] S. Miura, H. Goldenstein, K. Ohkubo, H. Sato, Y. Watanabe, T. Mohri, Mechanical and physical properties of $Ni_3Al$-based alloys with Cr carbides dispersion, Mater. Sci. Forum 561-565 (2007) 439–442.
[6] R.A. Varin, in: J. Martin (Ed.), Intermetallics: crystal structures, Elsevier, Amsterdam, The Netherlands 2007, pp. 235–238.
[7] S.P. Li, H.L. Luo, F. Di, X. Cao, X.E. Zhang, Abrasive performance of chromium carbide reinforced $Ni_3Al$ matrix composite cladding, J. Iron Steel Res. Int. 16 (2009) 87–91.
[8] S.P. Li, D. Feng, H.L. Luo, Microstructure and abrasive wear performance of chromium carbide reinforced $Ni_3Al$ matrix composite coating, Surf. Coat. Technol. 201 (2007) 4542–4546.
[9] K. Gong, H.L. Luo, D. Feng, C.H. Li, $Ni_3Al$-based intermetallic alloys as a new type of high-temperature and wear-resistance materials, J. Iron Steel Res. Int. 14 (2007) 21–25.
[10] K. Liu, Y.J. Li, J. Wang, In-situ reactive fabrication and effect of phosphorus on microstructure evolution of Ni/Ni-Al intermetallic composite coating by laser cladding, Mater. Des. 105 (2016) 171–178.
[11] H. Goldenstein, Y.N. Silva, H.N. Yoshimura, Designing a new family of high temperature wear resistant alloys based on $Ni_3Al$ IC: experimental results and thermodynamic modelling, Intermetallics 12 (2004) 963–968.
[12] W.S. da Silva, R.M. Souza, J.D.B. Mello, H. Goldenstein, Room temperature mechanical properties and tribology of NICRALC and stellite casting alloys, Wear 271 (2011) 1819–1827.
[13] S.Y. Zhu, Q.L. Bi, Y. Jun, W.M. Liu, Q.J. Xue, $Ni_3Al$ matrix high temperature self-lubricating composites, Tribol. Int. 44 (2011) 445–453.
[14] G. Cios, P. Bała, M. Stępień, K. Górecki, Microstructure of cast Ni-Cr-Al-C alloy, Arch. Metall. Mater. 60 (2015) 145–148.
[15] K. Gong, T.B. An, Z.F. Zhou, Z.L. Tian, C.H. Li, Study on wear behaviors of $Ni_3Al$/Cr-carbides cladding layer on high strength steel substrate, Adv. Mater. Res. 936 (2014) 1273–1282.
[16] K. Gong, Z.F. Zhou, P.W. Shum, H.L. Luo, Z.L. Tian, C.H. Li, Tribological evaluation on $Ni_3Al$-based alloy and its composites under unlubricated wear condition, Wear 270 (2011) 195–203.
[17] E. Bullock, M. McLean, D.E. Miles, Creep behaviour of a Ni-$Ni_3Al$-$Cr_3C_2$ eutectic composite, Acta Metall. 25 (1997) 333–344.
[18] K. Gong, H.L. Luo, D. Feng, C.H. Li, Wear of $Ni_3Al$-based materials and its chromium-carbide reinforced composites, Wear 265 (2008) 1751–1755.
[19] S.P. Li, H.L. Luo, X. Cao, G.R. Gu, X.E. Zhang, D. Feng, Microstucture and room-temperature wear-resistance of $Cr_3C_2/Ni_3Al$ composites, Rare Metal Mater. Eng. 37 (2008) 115–118.
[20] S.S. Li, M.L. Wu, L. Sun, L.W. Jiang, Y.F. Han, Fretting wear resistance of ATW $Cr_3C_2/Ni_3Al$ composite hardfacing on IC6SX, Mater. Sci. Forum 654-656 (2010) 532–537.
[21] H.Y. Yoshimura, H.N.Y. Matsubara, H. Goldenstein, WCI-white cast intermetallic compound-a new high temperature foundry material, Acta Microsc. 6 (Suppl.A) (1997) 174–175.
[22] A. Muñoz, M.A. Monge, B. Savoini, M.E. Rabanal, G. Garces, R. Pareja, $La_2O_3$-reinforced W and W-V alloys produced by hot isostatic pressing, J. Nucl. Mater. 417 (2011) 508–511.
[23] D. Božić, O. Dimčić, B. Dimčić, M. Vilotijević, S. Riznić-Dimitrijević, Modeling of densification process for particle reinforced composites, J. Alloys Compd. 487 (2009) 511–516.
[24] L.T. Chang, W.R. Sun, Y.Y. Cui, R. Yang, Influence of hot-isostatic-pressing temperature on microstructure, tensile properties and tensile fracture mode of Inconel powder compact, Mater. Sci. Eng. A 599 (2014) 186–195.
[25] R.Z. Vlasyuk, I.D. Radomysel'skii, V.P. Smirnov, A.A. Sotnik, Dissolution of $Cr_3C_2$ in a Nickel matrix during sintering I. Reaction of chromium carbide with nickel during solid-phase sintering, Powder Metall. Met. Ceram. 24 (1985) 356–360.
[26] S. Anthonysamy, K. Ananthasivan, I. Kaliappan, V. Chandramouli, P.R. Vasudeva Rao, C.K. Mathews, K.T. Jacob, Gibbs energies of formation of chromium carbides, Metall. Mater. Trans. A 27A (1996) 1919–1924.

[27] R.Z. Vlasyuk, V.B. Deimontovich, A.A. Mamonova, I.D. Radomysel'skill, Dissolution of the carbide $Cr_3C_2$ in an Iron matrix, Powder Metall. Met. Ceram. 20 (1981) 689–693.
[28] Y.L. Yuan, Z.G. Li, Effects of rod carbide size, content, loading and sliding distance on friction and wear behaviors of (Cr, Fe)$_7C_3$–reinforced α-Fe based composite coating produced via PTA welding process, Surf. Coat. Technol. 248 (2014) 9–22.
[29] J.A.R. Wesmann, N. Espallargas, Effect of atmosphere, temperature and carbide size on the sliding friction of self-mated HVOF WC-CoCr contacts, Tribol. Int. 101 (2016) 301–313.
[30] S.Y. Zhu, Q.L. Bi, J. Yang, W.M. Liu, Influence of Cr cotent on tribological properties of $Ni_3Al$ matrix high temperature self-lubricating composites, Tribol. Int. 44 (2011) 1182–1187.
[31] J. Yang, P.Q. La, W.M. Liu, J.Q. Ma, Q.J. Xue, Tribological properties of $Fe_3Al$-$Fe_3AlC_{0.5}$ composites under dry sliding, Intermetallics 13 (2005) 1184–1189.